15.4 The Effects of Thermodynamic Variability on Low-Level Baroclinity and Vorticity within Numerically Simulated Supercell Thunderstorms

Jeffrey Beck*
Christopher Weiss

Texas Tech University, Lubbock, Texas

1. INTRODUCTION

Idealized supercell modeling has provided immense insight into the dynamics of supercell thunderstorms. The dynamics and origin of mid-level rotation, as well as the evolution of low-level mesocyclogenesis have been the main areas of research of these studies (e.g., Weisman and Klemp 1982, 1984; Wicker and Wilhelmson 1995; Adlerman et al., 1999). While they have yielded important findings, these studies were initialized from the same thermodynamic conditions. The 20 May 1977 sounding from Del City, OK (or a minor variant) has been the benchmark sounding for these studies, yet it is well known that the environmental thermodynamic parameter space in which supercell thunderstorms can exist is much broader. Furthermore, observational research has found that the structure and dynamics of low-level features within supercells do not always follow the findings from these past idealized studies (e.g., Richardson et al., 2001; Dowell et al., 2002; Dowell and Bluestein, 2002a, 2002b; Beck et al., 2006).

The focus of this research is to explore the thermodynamic parameter space in which supercells exist in a more thorough fashion. The hypothesis of this research is that imposed variations in evaporational cooling, precipitation loading, and entrainment of environmental air will help explain the variance seen in observational studies, and ultimately lead to a better understanding of low-level baroclinity, vorticity, and their collective role in supercell dynamics.

* *Corresponding author address: Jeffrey Beck, Texas Tech University, Atmospheric Science Group, Department of Geosciences, Lubbock, TX, 79409; e-mail: j.beck@ttu.edu*

2. METHODS

Historical precedence of the 20 May 1977 sounding makes it a logical choice for a benchmark simulation for this study. Yet, in an idealized setting, it is preferable to use a control sounding that is free of minor temperature or moisture deviations, and is easily manipulated. Therefore, the Weisman and Klemp (1982, 1984) sounding, based on the 20 May 1977 case, was used (Fig. 1). Altering the analytical equations used to create the control sounding, variations in sub-cloud relative humidity, cloud-depth relative humidity, and freezing level were all made within the confines of the environmental space in which supercells have been shown to exist (Fig. 2).

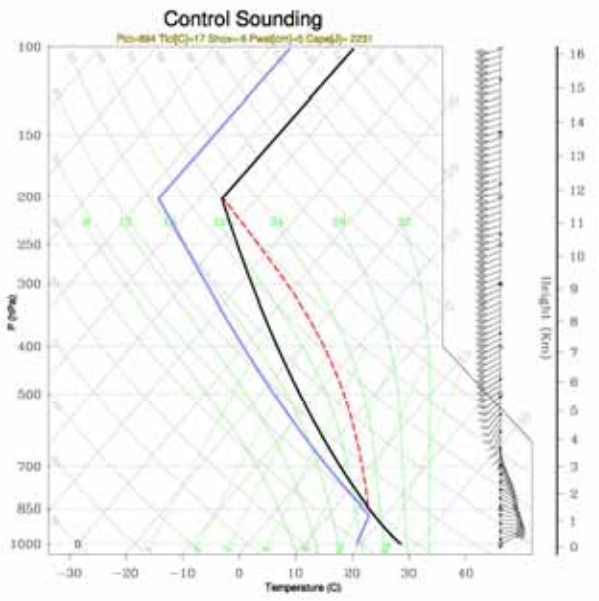

FIG. 1 – Control sounding adapted from the Weisman and Klemp (1982, 1984) atmospheric profile based on the 20 May 1977 Del City, OK sounding.

The quantity of each variation was assigned using actual proximity soundings from supercell events. Each of these altered thermodynamic profiles

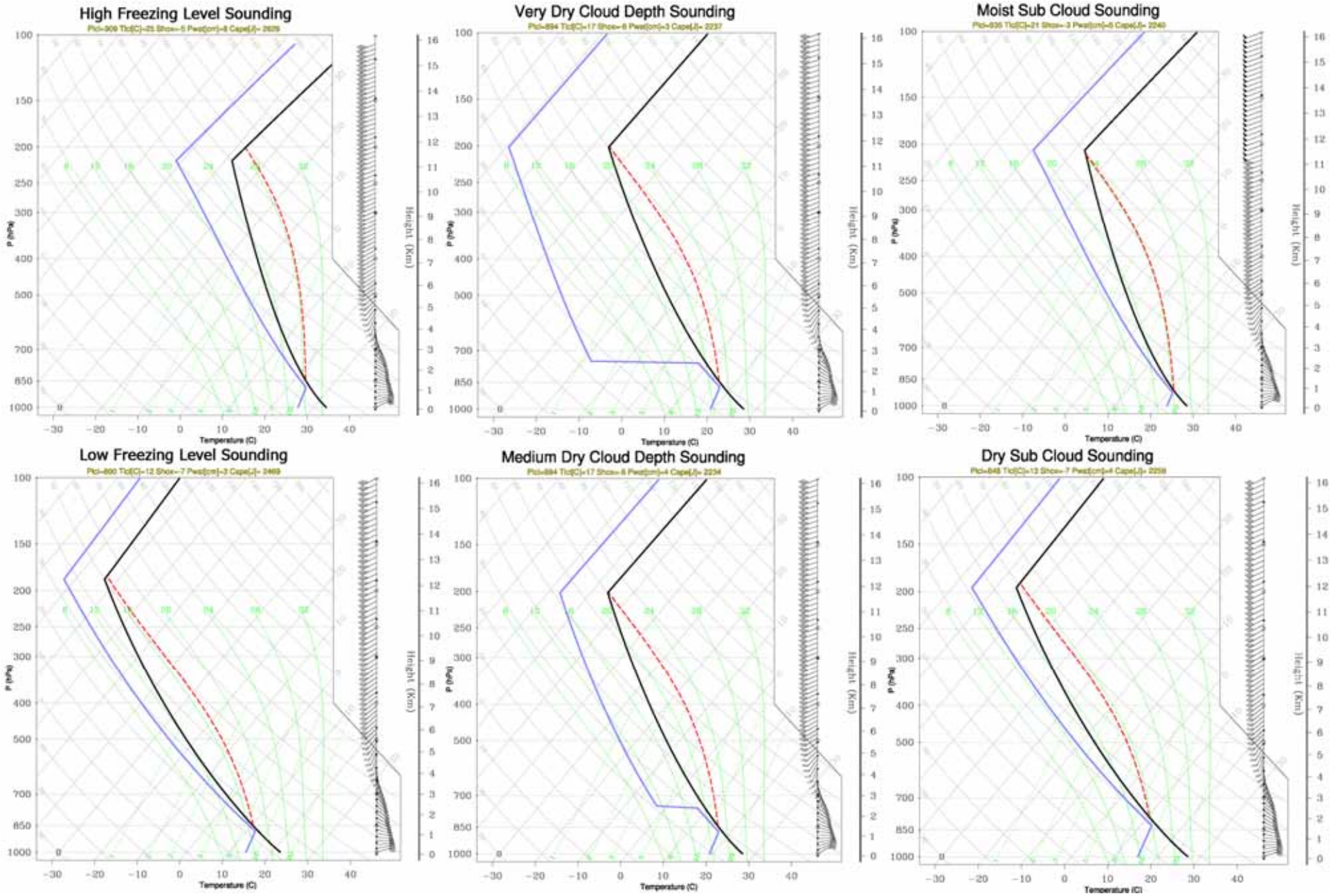

FIG. 1 – Skew-T diagrams of all the simulations (aside from the control, and those involving microphysical changes) conducted in the study.

successfully produced a supercell in model space, based on the magnitude of mid-level vertical vorticity and the structure of the storm. Rain intercept parameters were also altered in the microphysical scheme, based on previous modeling work by Gilmore et al. (2004a, 2004b).

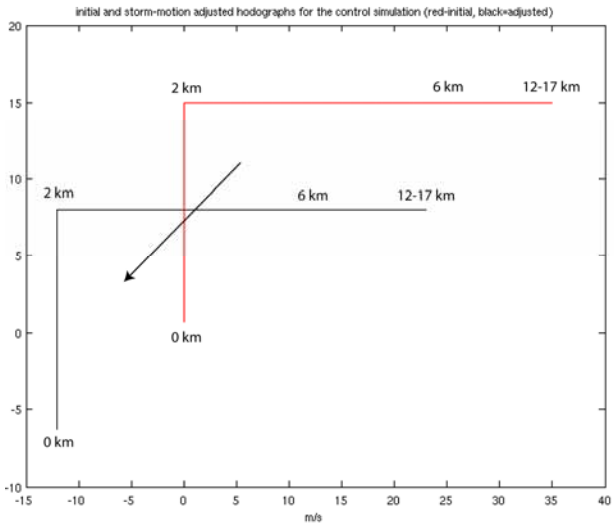

Fig 3. Hodographs for the control simulation. The initial hodograph in red, and the adjusted hodograph in black. Adjustment (using the control as an example) for each simulation was necessary to keep the storm from moving out of the domain (black arrow). All changes in wind speed with height are linear in nature.

The Weather Research and Forecasting (WRF) model was used to conduct these simulations at the National Center for Supercomputing Applications (NCSA). Each simulation had dimensions of 641 x 641 x 51 data points, with a horizontal grid spacing of 250 meters, and a vertically stretched grid spacing starting at 100 meters near the surface and ending at 1.5 km at the top of the domain (17 km AGL). The WRF Single Moment 6-Class (WSM6) microphysics package was chosen for this study, with an initial convective perturbation introduced for initialization. An "L-shaped" hodograph was chosen for each simulation (Fig. 3); similar to, but a variation from the hodographs used by Wicker (1996) and Klemp and Weisman (1983).

The convective available potential energy (CAPE) was held constant throughout each simulation in order to achieve approximately equal updraft buoyancy, isolating the effects of each thermodynamic variation in the experimental design.

Each simulation was run out to three hours to allow for the generation of storm-scale boundaries in proximity to the updraft/low-level mesocyclone. However, a number of the simulations had secondary outflow (from storm splits) that impacted the initial right-moving supercell after a period of time. In order to insolate the impacts of environmental parameters on boundaries generated by the primary storm, the analysis window for each simulation was terminated prior to any storm interaction.

3. PRELIMINARY FINDINGS

I. Control Simulation

In order to assess the variance in baroclinity/baroclinically induced horizontal vorticity, and the magnitudes of both vertical and horizontal vorticity between the simulations, thorough analysis of the control simulation is necessary. Based on the development and evolution of the control supercell, multiple low-level boundaries with varying degrees of baroclinity form within the time period analyzed.

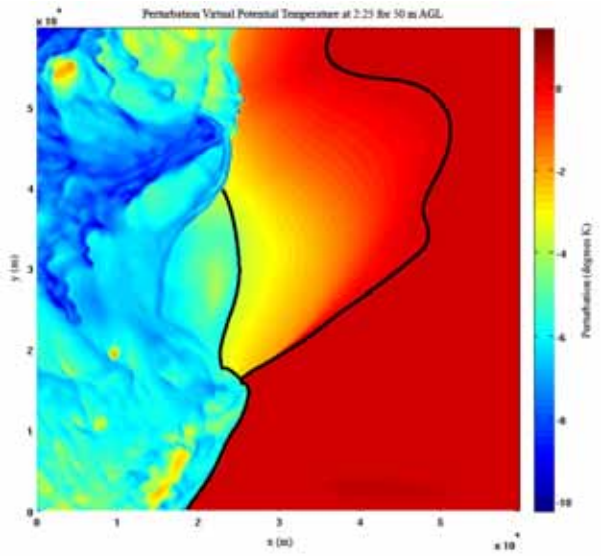

Fig. 4. A plot of perturbation virtual potential temperature (degrees K) at 2:25 for 50 m AGL. Black lines indicate boundaries that are discussed in the text.

A clearly defined rear-flank gust front is present early in the evolution of the storm. Furthermore, there is evidence of a forward-flank gust front, and a third, rapidly evolving boundary extending north from the low-level mesocyclone (Fig. 4). These

three boundaries are persistent throughout the lifetime of the storm.

The forcing appears to be different for each boundary. As equivalent potential temperature varies little, if at all, across the forward-flank gust front, it is clear that air on either side of the boundary originates from the same source (low-level inflow). Yet, the air behind the boundary is virtually cooler (Fig. 6). Therefore, it is likely that this baroclinic boundary is the result of cooling from the evaporation of inflow air from precipitation falling downshear of the updraft.

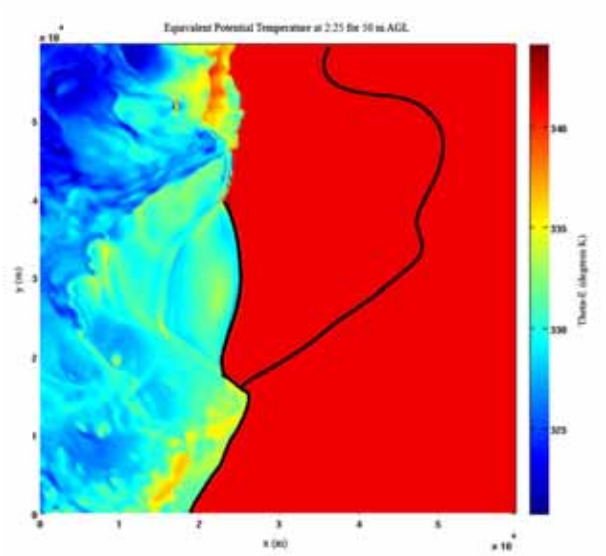

Fig 5. A plot of equivalent potential temperature (degrees K) at 2:25 for 50 m AGL. Black lines mark boundary locations.

The rear-flank gust front is forced strongly by high amounts of precipitation in the rear flank of the storm. Precipitation drag and evaporational cooling cause strong divergence near the surface and force a sharp gradient in virtual potential temperature. The boundary extending generally north from the mesocyclone is a rapidly evolving feature, in that it is the only boundary of the three that moves relative to the storm. It rotates counter-clockwise with time with the general circulation of the supercell, and its virtual potential temperature gradient weakens until it diminishes and is then replaced by a new boundary to the east. This succession of boundary replacements occurs early through midway into the life cycle of the storm, after which the boundary stabilizes. Backward trajectory analysis of air parcels on either side of the boundary show that it forms as a result of the differential descent of air within the forward flank (Fig. 6). Air east of the boundary comes from low-level inflow while, west of the boundary, air parcels descend from aloft (on the order of hundreds of meters). It is possible that this boundary is forced and dependent on downdraft pulses in the forward flank, due to its behavior.

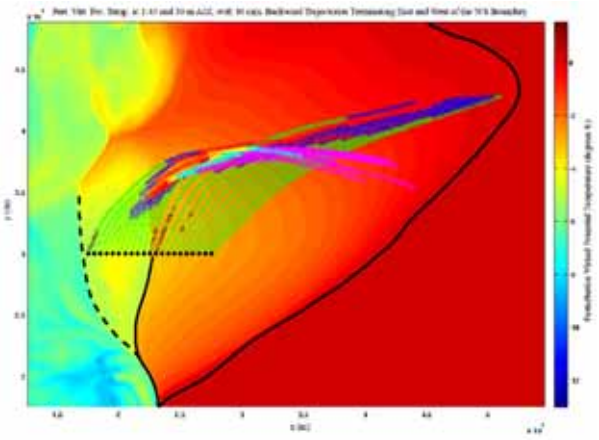

Fig 6. A plot of perturbation virtual potential temperature (degrees K) with backward trajectories terminating both east and west of the differential descent boundary for 1:45 at 50 m AGL. Colors of the trajectory points indicate elevation, where green is for parcels between 0.05 km AGL and 0.1 km AGL while magenta, the "highest" color, is for levels above 0.6 km AGL. Black lines mark boundary locations, while dashed lines mark decaying boundaries.

Trajectory analyses from the control simulation show that air parcels terminating in the first low-level mesocyclone generated by the storm originate solely north of the center of circulation. Backward trajectories terminating in the secondary low-level mesocyclone show that air originates from all areas west to east (through north) of the mesocyclone, with air passing along both the forward-flank gust front, the differential descent boundary, and the northern portion of the occluded rear-flank gust front. Vorticity budgets will be calculated to assess the impact of these boundaries on the development of the low-level mesocyclones.

II. Comparison Findings

One method of assessing the importance of environmental conditions in developing and evolving supercells is to analyze differences in vertical vorticity time-height (VVTH) plots for each simulation in the experimental design (Fig. 7).

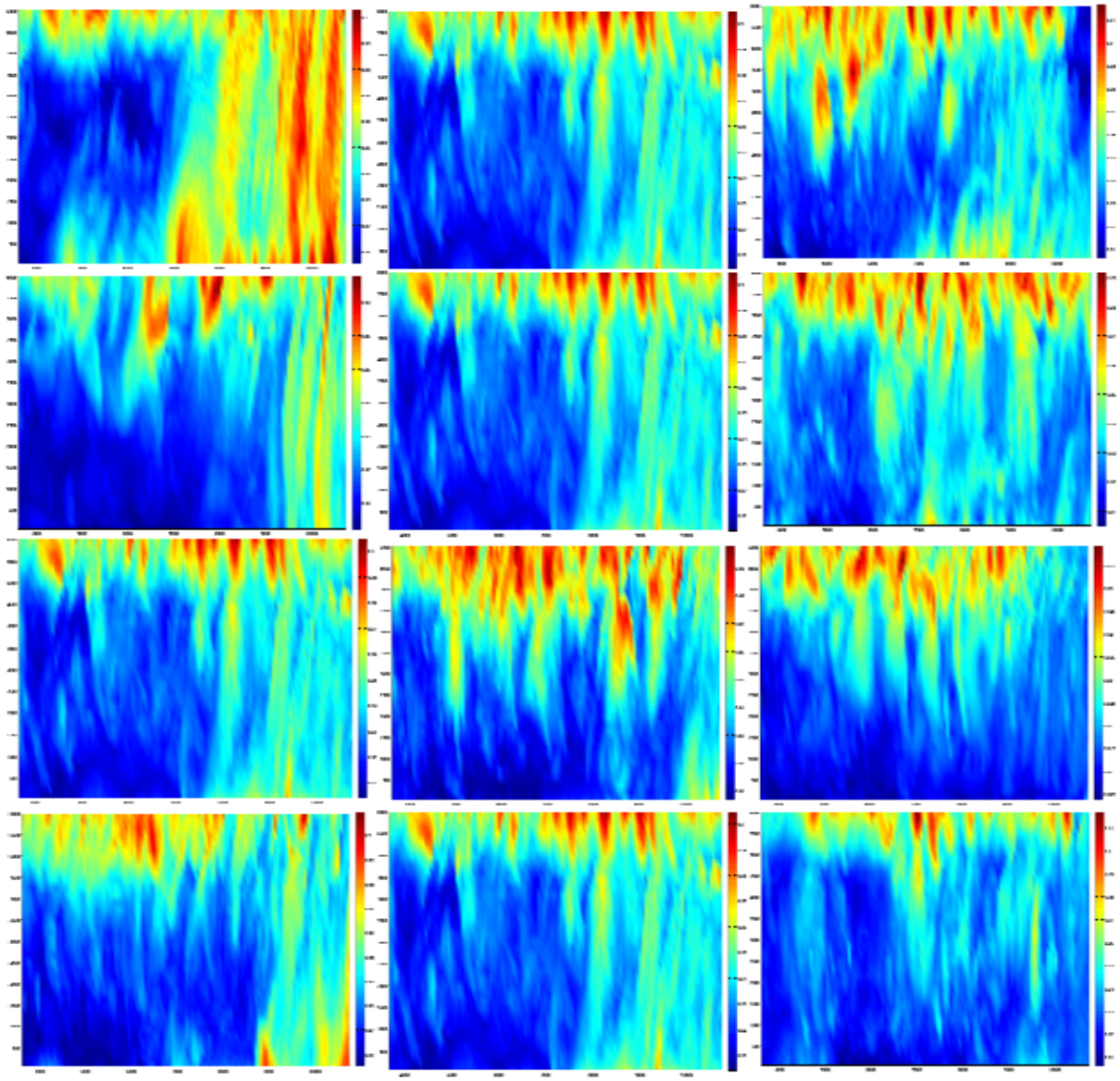

*Fig 7. Vertical Vorticity Time-Height (VVTH) plots for all simulations. Each plot has time in seconds (3600 to 10800 seconds) on the x-axis, with height in meters on the y-axis (surface to about 6 km AGL). Vertical vorticity is in inverse seconds. Starting in upper left-hand corner (**row one**: drop size distribution intercept values for rain: 8 x 10^5, 8 x 10^6 (control), 8 x 10^7; **row two**: sub-cloud mixing ratio:11 gkg^{-1} in boundary layer, 14 gkg^{-1} in boundary layer (control), 17 gkg^{-1} in boundary layer; **row three**: cloud-depth mixing ratio: control, medium dry, very dry; **row four**: freezing level: low freezing level, control, high freezing level).*

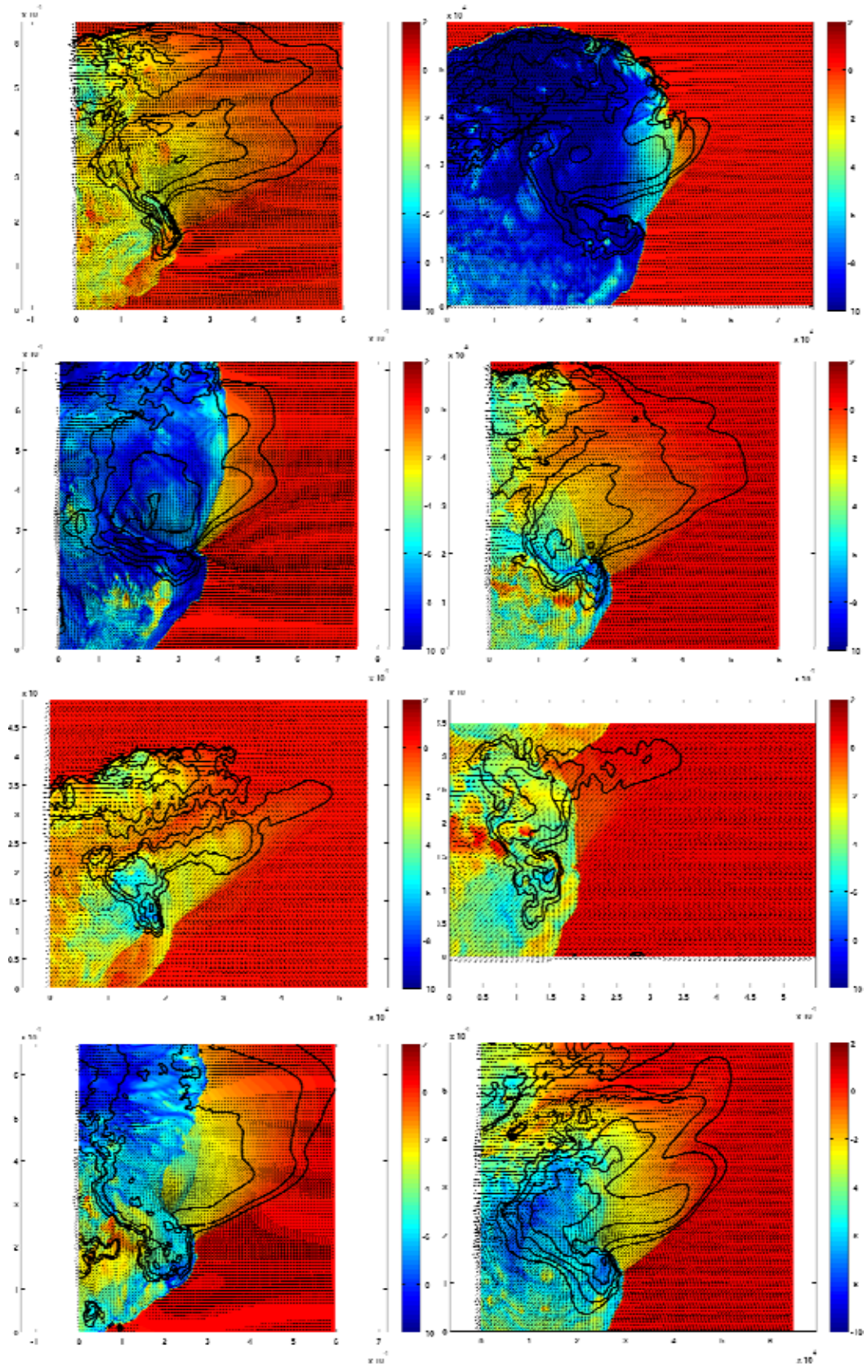

Fig 8. Perturbation virtual potential temperature (degrees K) plots for all simulations except the control at the time of the first low-level vertical vorticity maximum (low-level mesocyclone). Same rows as Fig. 7.

It is clear from these plots that changes in evaporational cooling, entrainment, and the freezing level have an effect on the strength, timing, height, and depth of vertical vorticity maxima. The mid- to upper-level mesocyclone appears to be least impacted by these changes. Most of the variability in the vertical vorticity is concentrated near the surface, highlighting the importance of environmental thermodynamic variability in understanding low-level supercell dynamics.

At the time of the first maxima in low-level vertical vorticity for each simulation, the variance in perturbation virtual potential temperature (Fig. 8) between the simulations is quite large, as is the timing of the first maxima in vertical vorticity. In one case, that of the very dry cloud-depth mixing ratio, there was no low-level mesocyclone development. Outflow in that case was too strong to sustain low-level development.

In general it can be seen that the three boundary scheme holds more or less for all simulations (Fig. 8), yet the strength of these boundaries varies at the time of the first low-level vertical vorticity maxima.

4. FUTURE WORK

In-depth analysis of the differences in low-level baroclinity between simulations will be conducted. Assessments of the strength of the gradients along each boundary for each simulation will be made in addition to frontogenetical forcing analyses. Backwards trajectories for all simulations will be compared to investigate origin locations for air parcels terminating in the low-level mesocyclones. These trajectories will also be useful for vorticity budget analyses to assess the amount of horizontal vorticity that is present, the amount being ingested by the low-level mesocyclone, and how much horizontal vorticity is being transferred to the air parcels by the boundaries through baroclinic processes.

The scope of this study is to assess the sign of the trend in baroclinity and vorticity between simulations and not necessarily to identify the type of function or slope of variability. Nonetheless, intermediate steps between the values of the environmental parameters will also be tested to ensure that no aliasing is occurring in the trend between simulations.

Finally, a more thorough literature review will be conducted to assess similarities and differences between the simulations and past observational and numerical-modeling studies.

5. ACKNOWLEDGEMENTS

The authors are grateful for the help and valuable input provided by the following: Drs. David Dowell, George Bryan, Morris Weisman, and Curtis Alexander.

6. REFERENCES

Adlerman, E. J., K. K. Droegemeier, and R. Davies-Jones, 1999: A numerical simulation of cyclic mesocyclogenesis. *J. Atmos. Sci.,* **56**, 2045-2069.

Beck, J. R., J. L. Schroeder, and J. Wurman, 2006: High-resolution dual-Doppler analyses of the 29 May 2001 Kress, Texas, cyclic supercell. *Mon. Wea. Rev.*, **134,** 3125-3148.

Dowell, D. C. and H. B. Bluestein, 2002a: The 8 June 1995 McLean, Texas, storm. Part I: Observations of cyclic tornadogenesis. *Mon. Wea. Rev*., **130**, 2626-2648.

Dowell, D. C. and H. B. Bluestein, 2002b: The 8 June 1995 McLean, Texas, storm. Part II: Observations of cyclic tornadogenesis. *Mon. Wea. Rev*., **130**, 2649-2670.

Dowell, D., Richardson, Y., Wurman, J**.**, 2002: Observations of the formation of low-level rotation: the 5 June 2001 Sumner County, Kansas, tornado, *21st Conference on Severe Local Storms*, San Antonio, American Meteorological Society.

Gilmore, M. S., J. M. Straka, and E. N. Rasmussen, 2004a: Precipitation and evolution sensitivity in simulated deep convective storms: Comparisons between liquid-only and simple ice and liquid phase microphysics. *Mon. Wea. Rev.*, **132**, 1897–1916.

Gilmore, M. S., J. M. Straka, and E. N. Rasmussen, 2004b: Precipitation uncertainty due to variations in precipitation particle parameters within a simple microphysics scheme. *Mon. Wea. Rev.,***132**, 2610–2627.

Klemp, J. B., and M. L. Weisman, 1983: The dependence of convective precipitation patterns on vertical wind shear. Preprints, *21st Conference on Radar Meteorology*, Edmonton, Alberta, Canada, Amer. Meteor. Soc., 44-49.

Richardson, Y., D. Dowell, and J. Wurman, 2001: High resolution dual-Doppler analyses of two thunderstorms during the pre-tornadogenesis and mature tornado stages, *30th Conference on Radar Meteorology*, Munich, American Meteorological Society.

Weisman, M. L. and J.B. Klemp, 1982: The dependence of numerically simulated convective storms on vertical wind shear and buoyancy. *Mon. Wea. Rev.* **110**, 504–520.

Weisman, M. L. and J.B. Klemp, 1984: The structure and classification of numerically simulated convective storms in directionally varying wind shears. *Mon. Wea. Rev.* **112**, 2479–2498.

Wicker, L. J., 1996: The role of near surface wind shear on low-level mesocyclone generation and tornadoes. *Preprints, 18th Conf. on Severe Local Storms,* San Francisco, CA, American Meteorological Society, 115-119.

Wicker, L. J. and R. B. Wilhelmson, 1995: Simulation and analysis of tornado development and decay within a three-dimensional supercell thunderstorm. *J. Atmos. Sci.* **52**, 2675–2703.